

Joint estimation of multi-target signal-to-noise ratio and dynamic states in cluttered environment

ISSN 1751-8784

Received on 17th August 2016

Revised 30th September 2016

Accepted on 11th October 2016

E-First on 17th November 2016

doi: 10.1049/iet-rsn.2016.0416

www.ietdl.org

Seung-Hwan Bae¹, Jongyoul Park¹, Kuk-Jin Yoon² ✉¹*SW-Content Research Laboratory, Electronics and Telecommunications Research Institute, 218 Gajeong-ro, Yuseong-Gu, Daejeon, 34129, South Korea*²*School of Information and Communications, Gwangju Institute of Science and Technology, 123 Cheomdan-Gwagiro, Buk-Gu, Gwangju, 61005, South Korea*✉ E-mail: kjyoon@gist.ac.kr

Abstract: In this study, the authors consider a multi-target tracking (MTT) problem in a cluttered environment. Due to the difficulty of the problem, the methods relying only on spatial information such as range, bearing and Doppler velocity can be unreliable. To overcome this, they additionally exploit the amplitude information, commonly provided by radar and sonar, for MTT. However, the usage of amplitude information is not straightforward because the signal-to-noise ratio (SNR) should be known in advance or estimated at the same time. To this end, they first propose a novel SNR estimation algorithm based on a maximum a posteriori approach, which helps the tracker to exploit the amplitude information effectively. Based on the estimated SNR, they then propose a complete framework for MTT, which is mainly composed of data association and track state update parts. They extensively evaluate the proposed system in a series of challenging scenarios, and the experimental results verify the effectiveness and robustness of the authors' methods.

1 Introduction

Automated multi-target tracking (MTT) has been applied to various applications such as radar-based tracking [1, 2] and visual object tracking [3, 4]. In general, this problem is formulated to find states of multiple targets using a set of sensor measurements. In most cases, the measurement origin is also unknown since a sensor usually receives mixed signals reflected from both targets and random clutter. Thus, to successfully solve the MTT problem, a data association process is required, which would be able to correctly associate measurements with the corresponding tracks.

This task can be simply performed using greedy algorithms such as the nearest neighbourhood [5] or the strongest neighbour [6] data association. However, they do not properly consider the case in which measurements of multiple targets are scattered. To find optimal solution for the joint track-to-measurement assignment through single-frame and multi-frame searches, joint probabilistic data association [5] and multiple hypothesis tracking (MHT) [7] have been proposed. However, they incur large computational costs as the number of possible joint assignments combinatorically increases due to the number of tracks and measurements. Recently, in an attempt to alleviate this complexity, linear multi-target integrated probabilistic data association (LMIPDA) [8] has been developed. However, incorrect association is often made when targets are closely spaced or clutter is densely distributed in the target vicinity. In these situations, exploiting only spatial information [5, 7–9] is not sufficient for discriminating between target and clutter measurements.

Since practical sensors such as a radar and a sonar provide amplitude information as well as spatial properties, the amplitude can be utilised as an additional feature. However, using amplitude in filtering to estimate the states of targets might also be challenging because of the difficulty of designing an explicit model that describes the direct relationship between target states, e.g. positions and velocities, and amplitude measurement. Therefore, instead of directly exploiting amplitude for state estimation, it is more common to utilise it in the data association process, based on the practical assumption that the signal amplitude returned from a target is stronger than that returned from clutter [2, 10–13].

Based on this finding, data association methods using the amplitude information have been proposed for more accurate association. An extension [12] of probabilistic data association and the highest probabilistic data association [10] have been developed for single object tracking in a cluttered environment. In addition, amplitude has been incorporated into MHT [13] and Viterbi data association [11]. Recently, for tracking multiple targets with different signal-to-noise ratios (SNRs), the amplitude was also incorporated into a framework of finite set statistics [2]. In a similar manner, we make use of the amplitude feature to enhance description ability when associating between tracks and measurements.

As a common way of utilising the amplitude for the association, the amplitude likelihood function of a target is calculated based on the probability density function of the amplitude [2, 6, 11–13]. In general, the density is modelled by the Rayleigh distribution [2, 12] with respect to the SNR and received amplitude based on the assumption that a received signal is Rayleigh faded. This model is appropriate for scan-to-scan slow fluctuation (Swierling I) and pulse-to-pulse fast fluctuation (Swierling II) [14, 15], which are mostly used when changes in target orientation lead to large SNR changes.

In most previous works [6, 11–13], for evaluating the amplitude likelihood function, it is assumed that target SNRs are known and fixed during tracking. However, the SNR information may not be available in many practical applications. Even though knowledge of the (initial) SNR is provided, the SNR should be updated due to its fluctuation caused by the following reasons: (i) the received signal of the target is faded by propagation and attenuation through a medium [12]; (ii) the returns of most targets are composed of the sum of reflected rays from individual scattering points [2, 16]; and (iii) the aspect angle of the target is changed by the target motion [14]. To resolve the limitations of using the amplitude feature, we propose a novel SNR estimation method based on a maximum a posteriori (MAP) inference.

If the target SNRs are estimated, we can then employ amplitude in conjunction with the spatial feature for MTT. In this study, we designed a complete MTT system that uses both kinematic and non-kinematic features effectively, which consists of data association and track state update parts. In particular, we extend the two-step

recursive procedure (i.e. prediction and update) of conventional particle filtering [17] to a three-step procedure including a measurement selection step, which allocates one of the measurements to each sample using the (posterior) association probability evaluated by the association part. As a result, we can improve the robustness of the filtering part by updating the sample weights with associated measurements while reducing its complexity.

To evaluate the SNR estimation method, we constructed a practical experimental setup and extensively evaluated its performance. Furthermore, to prove the effectiveness and robustness of our MTT system, we implemented several MTT systems using different association methods, and compared their performance for three MTT scenarios and a challenging benchmark dataset.

2 Probabilistic amplitude information modelling

In this section, we first present probabilistic amplitude models for target and false alarm (or clutter), which can be expressed with amplitude and its SNR. As previously mentioned, in designing the models, most of the previous methods using amplitude [6, 11–13] assume that the SNR is known and fixed. Practically, however, it is difficult to know the target SNR in advance since it often randomly fluctuates according to signal fading [12], interference from other signals [2, 16] from other targets and clutter; and the change of the target aspect angle [14]. To overcome this limitation, we propose a method for estimating unknown target SNRs based on MAP inference.

2.1 Amplitude likelihood models

Let us assume that amplitude is the output of a bandpass matched filter that has an envelope detector attached. In this case, the probability density of the amplitude a follows a Rayleigh distribution [For clarity, the set, matrix, vector, and scalar are denoted by blackboard bold font, upper boldface, boldface, and standard italic types, e.g. \mathbb{A} , \mathbf{A} , \mathbf{a} , a], as described in [12, 16]. The amplitude probability density of false detections (or clutter) can be expressed as

$$p_c(a) = \frac{a}{\sigma^2} \cdot \exp\left(\frac{-a^2}{2\sigma^2}\right), \quad a \geq 0, \quad (1)$$

where σ^2 is the variance (or power) of the in-phase and quadrature components (x_s, y_s) [12] of the narrow band noise coming out of the matched filter, where each component is assumed to be Gaussian, but independent of each other. Here, $x_s, y_s \sim \mathcal{N}(0, \sigma^2)$ and the amplitude a is defined as $a = \sqrt{x_s^2 + y_s^2}$. Note that the amplitude density function is the representation of the power (σ^2) of each component. However, as discussed in [18], in the narrow band filter, the amplitude density function of the noise is modelled with the average (or total) noise power σ_{noise}^2 rather than the power σ^2 of the component since the receiver bandwidth-to-centre frequency ratio is usually small. Thus, we reformulate it with average noise power σ_{noise}^2 , where $\sigma_{\text{noise}}^2 = 2\sigma^2$:

$$p_0(a) = \frac{2a}{\sigma_{\text{noise}}^2} \cdot \exp\left(\frac{-a^2}{\sigma_{\text{noise}}^2}\right), \quad a \geq 0, \quad (2)$$

We also assume that the background noise is normalised as in [2, 12]. This means that the variance of the noise (2) is $\sigma_{\text{noise}}^2 = 1$, and the expected noise power N_0 is unity as

$$N_0 = E[a^2] = \int_0^\infty a^2 p_0(a) da = 1. \quad (3)$$

We then define the expected (or mean) SNR [The SNR is represented in log scale: SNR (dB) = $10\log_{10}(d)$.] $d = S/N_0$, where S is the signal power and d can be treated as the expected target

signal power because $N_0 = 1$. In addition, we consider a slow Rayleigh fading amplitude-modulated narrowband signal in the presence of narrowband noise. In this case, the signal returned from the target is expressed as the sum of the transmitted signal and the narrow band noise. Also, as described above, the noise has the normal distribution with zero mean and unit variance (i.e. $\sigma_{\text{noise}}^2 = 1$). Therefore, the amplitude density function of a target follows Rayleigh distribution with the variance $1+d$ (i.e. the signal-plus-noise to noise ratio):

$$p_1(a, d) = \frac{2a}{1+d} \cdot \exp\left(\frac{-a^2}{1+d}\right). \quad (4)$$

However, to evaluate the signal power S from the target amplitude distribution (4), we need to estimate the expected target SNR d because

$$S = E[a^2] = \int_0^\infty a^2 p_1(a, d) da. \quad (5)$$

Let us next consider the case in which the amplitude a exceeds a detection threshold DT , i.e. $a \geq DT$. Then, the amplitude density of the target becomes

$$p_1^{\text{DT}}(a, d) = \frac{1}{P_D} p_1(a, d) = \frac{2a}{1+d} \cdot \exp\left(\frac{DT^2 - a^2}{1+d}\right), \quad a \geq DT, \quad (6)$$

where the target detection probability P_D used for normalisation is calculated as

$$P_D = \int_{DT}^\infty p_1(a, d) da = \exp\left(\frac{-DT^2}{1+d}\right). \quad (7)$$

Otherwise the amplitude probability density of false alarms is expressed from (2)

$$p_0^{\text{DT}}(a) = \frac{1}{P_{\text{FA}}} p_0(a) = 2a \cdot \exp(DT^2 - a^2), \quad a \geq DT, \quad (8)$$

where the clutter detection probability P_{FA} is given as

$$P_{\text{FA}} = \int_{DT}^\infty p_0(a) da = \exp(-DT^2). \quad (9)$$

When the target SNR d is known, the amplitude likelihoods of both the target and clutter can then be computed as

$$g_a^{\text{DT}}(a|d) = p_1^{\text{DT}}(a, d), \quad (10)$$

$$c_a^{\text{DT}} = p_0^{\text{DT}}(a). \quad (11)$$

Once the likelihood functions $g_a^{\text{DT}}(a|d)$ and c_a^{DT} are obtained, we utilise the amplitude information to discriminate different targets and/or clutter using the likelihoods. A tracking method using this amplitude information will be discussed in Section 3. To exploit the amplitude in the general case without the assumption of the known SNR, we present a novel SNR estimation method based on MAP inference in the following section.

2.2 MAP inference for unknown SNR estimation

2.2.1 SNR estimation: To estimate an unknown SNR, a large number of amplitude measurements are usually required as proved by Clark *et al.* [2] with Cramer-Rao lower bound. Therefore, rather than inferring the target SNR with an instant amplitude measurement a_k^τ of target τ at scan k , we estimate it with a set of amplitude measurements stacked during Δ scans.

Let us denote the stacked amplitude measurements from time $k - \Delta$ to time k as $a_{k-\Delta:k}^r$. The MAP problem of finding an optimal SNR with respect to the collection of amplitudes $a_{k-\Delta:k}^r$ can be modelled by

$$\begin{aligned} \hat{d}_k^r &= \arg \max_d \prod_{a^r \in a_{k-\Delta:k}^r} p(a^r, d), \quad d \geq 0, \\ &= \arg \max_d \prod_{a^r \in a_{k-\Delta:k}^r} p(a^r | d) p(d), \\ &= \arg \max_d \sum_{a^r \in a_{k-\Delta:k}^r} \log(p(a^r | d)) + \log(p(d)), \end{aligned} \quad (12)$$

where the first likelihood term $p(a^r | d)$ is given by (10). To design the prior term $p(d)$, we consider the following two cases:

- *Case 1:* no previous knowledge of the SNR is available.
- *Case 2:* an initial (or previously estimated) SNR is provided, but it should be updated due to its random fluctuation.

In the first case, we consider that the SNR can be any value within any boundary $[d_1, d_2]$, and then the prior $p(d)$ can be modelled using the uniform distribution as follows:

$$p(d) = \begin{cases} \frac{1}{d_2 - d_1}, & d_1 \leq d \leq d_2, \\ 0, & \text{otherwise.} \end{cases} \quad (13)$$

The MAP problem (12) can be reformulated with the prior distribution (13)

$$\hat{d}_k^r = \arg \max_d \sum_{a^r \in a_{k-\Delta:k}^r} \log(p(a^r | d)) + \log(c), \quad c = \frac{1}{d_2 - d_1}. \quad (14)$$

Since c is constant, the MAP problem (14) can be transformed into the maximum likelihood (ML) estimation:

$$\hat{d}_k^r = \arg \max_d \sum_{a^r \in a_{k-\Delta:k}^r} \log(p(a^r | d)). \quad (15)$$

In the second case, we consider that the SNR is randomly fluctuated in the vicinity of the initial (or previously estimated) SNR \hat{d}_{k-1}^r . We model the prior $p(d)$ using the Gaussian random walk having the mean \hat{d}_{k-1}^r and variance σ_d^2 as follows:

$$p(d) = \mathcal{N}(d; \hat{d}_{k-1}^r, \sigma_d^2), \quad \hat{d}_k^r \geq 0. \quad (16)$$

By substituting the prior of (12) with (16), we obtain the following objective function:

$$\begin{aligned} \hat{d}_k^r &= \arg \max_d \sum_{a^r \in a_{k-\Delta:k}^r} \log(p(a^r | d)) + \log(c), \\ c &= \mathcal{N}(d; \hat{d}_{k-1}^r, \sigma_d^2). \end{aligned} \quad (17)$$

Next, the optimisation problems (15) or (17) can be considered as nonlinear least-squares problems; standard methods such as the Gauss–Newton and Levenberg–Marquardt [19] can thus be applied to solve them. In this paper, we exploit the Levenberg–Marquardt method.

2.2.2 Discussion: In many practical scenarios, we can effectively estimate the SNR of a target by using both ML (15) and MAP (17) methods. Once we find the initial SNR of a target by solving (15), we can sequentially update its SNR at each scan by solving (17) with the previous estimates.

For (15) and (17), we can use different scan sizes Δ . When no previous knowledge of the SNR is available in (15), we need many amplitude measurements to estimate it. However, when the previous SNR value is given in (17), we can find the optimal SNR value with only few amplitudes since the optimal value is near the previous estimate. In our experiment, we set $\Delta = 10$ and $\Delta = 5$ when solving (15) and (17), respectively.

Although we can solve (15) and (17) without the SNR boundary $[d_1, d_2]$, we can find a solution more efficiently by restricting the searching space within the boundary. The SNR boundary can be any values depending on applications and experimental environments. In this work, we set the minimum and maximum values to $d_1 = 1(0 \text{ dB})$ and $d_2 = 1000(30 \text{ dB})$ as in [2].

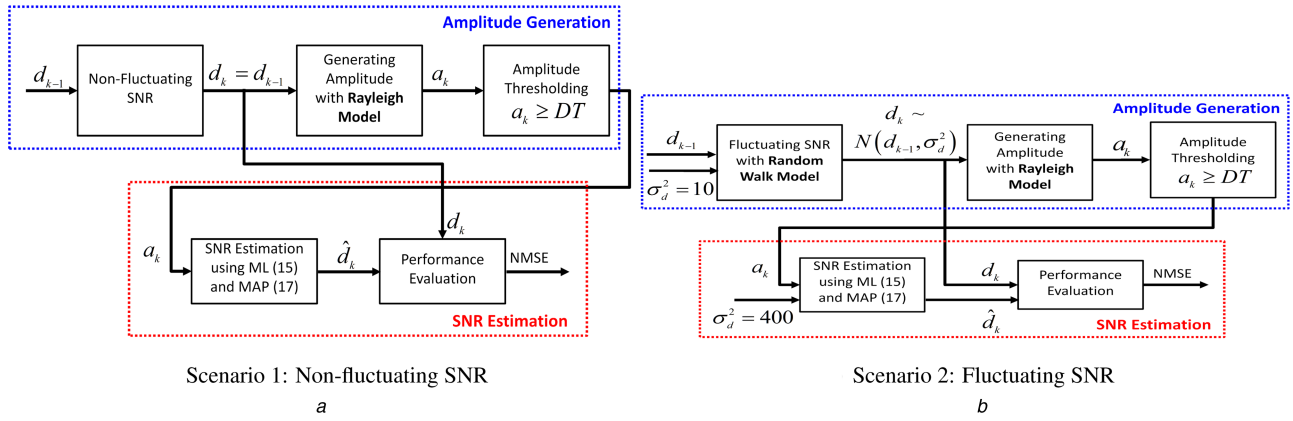
2.2.3 Evaluation: To verify the effectiveness of the proposed SNR estimation methods, we constructed an evaluation scheme with two different experimental scenarios as shown in Fig. 1.

- *Scenario 1:* There are six targets having various initial SNRs ranging from 7 to 12 dB and their SNRs are constant during 500 scans.
- *Scenario 2:* There are six targets having various initial SNRs ranging from 7 to 12 dB, but their SNRs fluctuate within the boundary range $[0 \text{ dB } 18 \text{ dB}]$ during 500 scans. At each scan, their fluctuations are modelled by the Gaussian random walk with variance $\sigma_d^2 = 10$ using (16).

When SNR is very high, the amplitude returned from the target can also be much higher than the clutter amplitude. Therefore, in both scenarios, we set the mean SNRs of the targets during 500 scans to be less than 16 dB since the estimation problem of the high target SNR (i.e. more than 20 dB) is not difficult.

In addition, in the most practical cases, target and clutter amplitude measurements exist together. The number of clutter measurements is closely related to the detector threshold DT . As discussed in [5], the average number of clutter measurements $E[N_{\text{FA}}]$ can be modelled by the function of the false alarm P_{FA} (9) and the number of resolution cells N_c : $E[N_{\text{FA}}] = P_{\text{FA}} N_c$. Furthermore, we assume that the target amplitude is detected according to the detection probability P_d (7). Note that both the detection probabilities P_{FA} and P_d are determined by the target SNR d and the threshold DT . For instance, the detection probability increases as the SNR d becomes high. Otherwise, the probability decreases. Also, we can remove a lot of false alarms using a high threshold DT . However, missing detection frequently occurs in return [In our experiment, we change the detection threshold DT from 1 to 6 dB, and set the number of resolution cells with $N_c = 400$ as in [5]. As a result, ranges of P_d and $E[N_{\text{FA}}]$ are $[0.071 \text{ } 0.976]$ and $[0 \text{ } 82]$, respectively.]

Once each true target SNR d_k is determined at each scan k in both scenarios as described above, we obtain an amplitude measurement set A_k consisting of a target and N_{FA} clutter amplitude measurements which are generated using Rayleigh distributions (6) and (8), respectively. Here, we filter out the amplitudes below a threshold DT before SNR estimation. With the set of thresholded amplitude measurements, we estimate the target SNR using the ML (15) and MAP (17) methods. In scenario 1, for the SNR estimation, the amplitudes are stacked during 10 scans ($\Delta = 10$). On the other hand, in scenario 2, we first find the initial SNR value with stacked amplitudes during 10 scans ($\Delta = 10$), and then we sequentially estimate it with stacked amplitudes during a reduced number of scans ($\Delta = 5$). In both estimation methods, the likelihood term is computed using the thresholded Rayleigh distribution (6) with the DT . Here, it is worth noting that we set the variance $\sigma_d^2 = 400$ when solving (17), which is significantly different from the true variance $\sigma_d^2 = 10$ used to generate the target SNR. From this experimental setup, we demonstrate that our method is not sensitive to the setting of the variance. For quantitative evaluation, we calculate the normalised mean square



d_k : True target SNR \hat{d}_k : Estimated SNR σ_d^2 : SNR variance
 a_k : Amplitude NMSE: Normalized Mean Square Error

Fig. 1 Evaluation schemes of the proposed SNR estimation
 (a) Scenario 1: Non-fluctuating SNR, (b) Scenario 2: Fluctuating SNR

errors (NMSEs) [20] between true d_k and estimated \hat{d}_k SNRs based on 500 Monte Carlo runs.

Table 1 compared the NMSEs of the ML and MAP estimation methods for various target SNRs and thresholds. Although the MAP method with $DT=2$ provides a better error rate in most cases, there is only slight difference in the performance of the ML and MAP methods. In some cases, the NMSEs of the ML method are better than those of the MAP method due to the large difference between the true variance $\sigma_d^2 = 10$ and the variance $\sigma_d^2 = 400$ used for MAP estimation.

Fig. 2 shows the SNR estimation results obtained using the MAP method with various thresholds. For scenario 1 shown in Figs. 2a–c, the estimates asymptotically approach the true SNRs as the number of scans increases. Furthermore, the estimates very rapidly reach the true SNR when the target SNR increases. Figs. 2d–f show the estimation results for fluctuating SNRs. We also confirm that using $DT=2$ produces the best estimation results. These results prove that the proposed SNR estimation methods can accurately estimate target SNRs with only amplitude measurements regardless of SNR fluctuation.

Once the unknown SNR parameter is estimated using the proposed method, we combine it into an MTT system to improve the association accuracy between tracks and measurements in a cluttered environment, as discussed in Section 3.3. More specifically, the estimated SNR \hat{d}_k^τ is used for the likelihood

evaluation (22) in the posterior association (20). In the following section, we present our MTT system, which uses SNR information.

3 MTT with spatial and amplitude information

In this section, we present a robust MTT system that uses the spatial and amplitude information.

3.1 Overall framework

Fig. 3 shows the overall framework of the proposed system. As an input, a set of measurements \mathbb{Z}_k containing spatial and amplitude measurements are given, the track components $\{\Omega_k^\tau\}_{\tau=1}^{M_k}$ and the track existence probability $\{P(\chi_k^\tau | \mathbb{Z}^k)\}_{\tau=1}^{M_k}$ of all M_k tracks are recursively updated in the proposed system. Here, the components of each track comprise N particles $\mathbf{x}_k^{n,\tau}$ with weights $w_k^{n,\tau}$, and the updated SNR d_k^τ , i.e. $\Omega_k^\tau = \{\{\mathbf{x}_k^{n,\tau}, w_k^{n,\tau}\}_{n=1}^N, d_k^\tau\}_{\tau=1}^{M_k}$. χ_k^τ is the event that the track τ exists in surveillance volume.

Each step in the framework can be briefly summarised as follows: In the measurement selection step, given a set of measurements \mathbb{Z}_k , we select validated measurements \mathbb{Z}_k^τ for existing tracks using the gating technique and amplitude thresholding. In the SNR estimation step, we then estimate the

Table 1 Performance evaluation with NMSEs for both scenarios (1 and 2). For each metric, the best results are marked in bold

		Target SNR								Target SNR					
		7 dB	8 dB	9 dB	10 dB	11 dB	12 dB	Method	Threshold (DT), dB	7 dB	8 dB	9 dB	10 dB	11 dB	12 dB
Scenario 1															
ML (15)	1	0.439	0.501	0.558	0.595	0.636	0.681	MAP (17)	1	0.441	0.505	0.565	0.604	0.650	0.700
	2	0.302	0.259	0.225	0.201	0.180	0.165		2	0.233	0.242	0.161	0.131	0.108	0.087
	3	0.702	0.535	0.427	0.352	0.291	0.252		3	0.916	0.440	0.275	0.210	0.147	0.111
	4	1.116	0.786	0.645	0.535	0.419	0.333		4	2.261	1.088	0.562	0.353	0.208	0.144
	5	2.296	1.307	0.952	0.767	0.604	0.487		5	5.900	2.970	1.295	0.681	0.371	0.222
	6	8.290	3.413	1.740	1.076	0.837	0.761		6	10.638	7.457	3.915	1.789	0.884	0.477
Scenario 2															
ML (15)	1	0.827	0.906	0.850	0.928	0.956	0.909	MAP (17)	1	0.883	1.002	0.896	0.994	1.025	0.992
	2	0.260	0.494	0.497	0.191	0.269	0.373		2	0.224	0.535	0.402	0.132	0.212	0.388
	3	0.356	0.984	0.758	0.254	0.379	0.515		3	0.322	1.129	0.524	0.147	0.269	0.496
	4	0.437	1.292	1.069	0.308	0.498	0.687		4	0.396	1.774	1.119	0.191	0.619	0.642
	5	0.558	1.696	1.360	0.409	0.750	1.042		5	0.483	2.333	1.954	0.325	1.029	0.996
	6	0.791	2.061	1.956	0.548	1.401	1.431		6	0.623	2.936	2.833	0.485	1.400	1.404

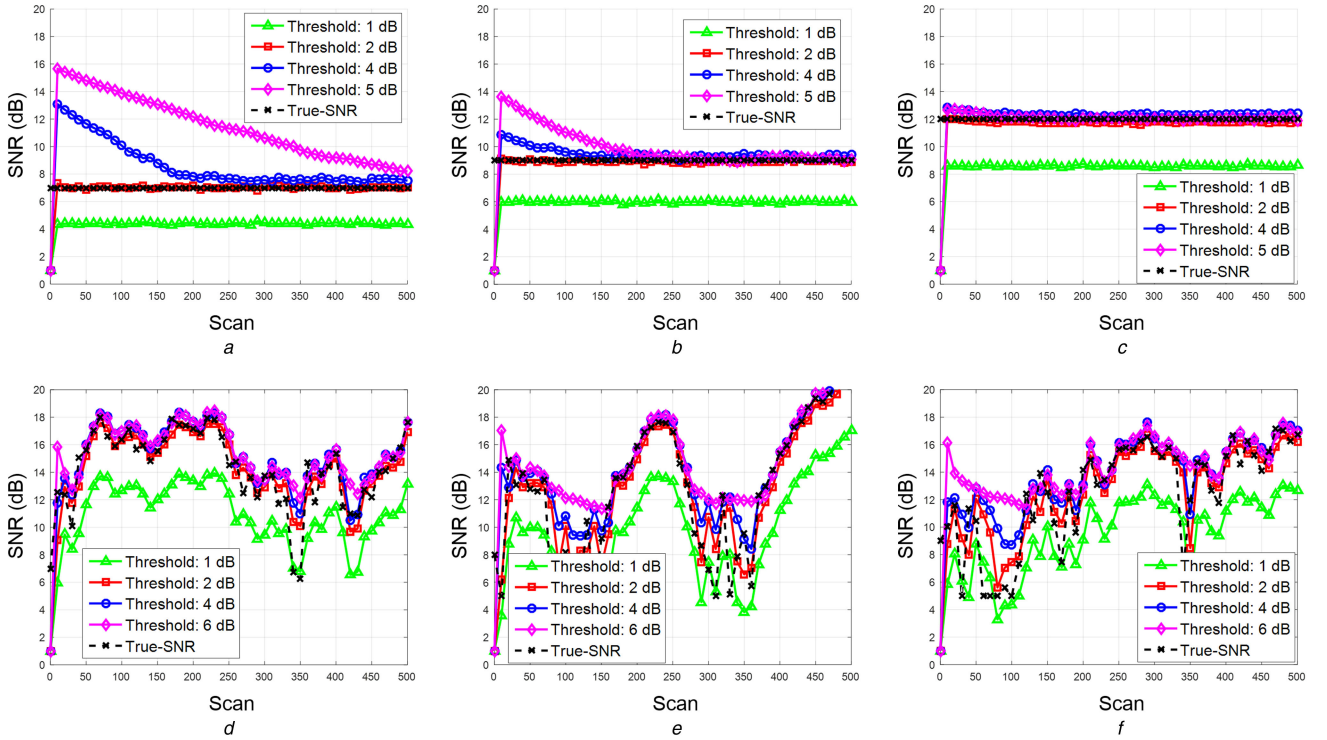


Fig. 2 SNR estimation results using the MAP estimation (17) for targets with different SNRs and thresholds. black dotted lines represent the true SNRs of targets and the coloured lines with different markers represent the estimation results
(a) Scenario 1 and target SNR 7 dB, (b) Scenario 1 and target SNR 9 dB, (c) Scenario 1 and target SNR 11 dB, (d) Scenario 2 and mean of target SNR 15.1 dB, (e) Scenario 2 and mean of target SNR 15.3 dB, (f) Scenario 2 and mean of target SNR 13.9 dB

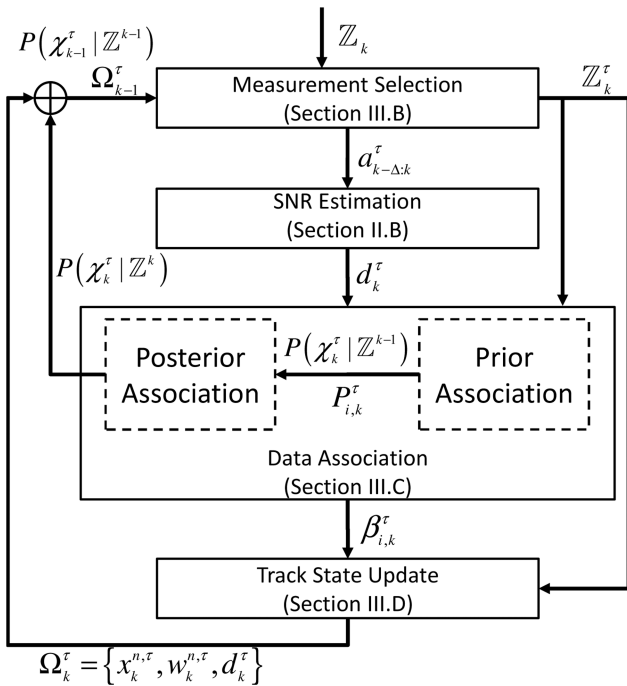


Fig. 3 Overall framework of the proposed MTT system during one recursion cycle

SNRs of targets d_k^τ with amplitude sets $a_{k-\Delta:k}^\tau$ using the proposed SNR estimation method. In data association, we associate \mathbb{Z}_k^τ with existing tracks using spatial and amplitude likelihood models. This procedure updates the posterior association probability $\beta_{i,k}^\tau$ and the posterior existence probability $P(\chi_k^\tau | \mathbb{Z}_k^\tau)$. In the track state update step, we update the states of all tracks with the posterior association probability $\beta_{i,k}^\tau$ via particle filtering. For more details, refer to the corresponding sections.

3.2 Measurement selection

In general, the measurement set obtained at one scan is composed of many measurements originated from multiple targets and clutter [5, 16].

Let us denote a set of measurements at scan k as $\mathbb{Z}_k = \{z_{i,k}\}_{i=1}^{m_k}$, where the measurement vector $z_{i,k} = [r_{i,k}, \theta_{i,k}, a_{i,k}]^T = [y_{i,k}, a_{i,k}]^T$ is composed of range $r_{i,k}$, bearing $\theta_{i,k}$ and amplitude $a_{i,k}$ elements. As in probabilistic data association filter (PDAF) [5], we exploit the gating technique to reduce matching combinations between tracks and measurements. Using the gating technique, m_k^τ validated measurements in the gate of the track τ is determined by

$$\mathbb{Z}_k^\tau = \{z_{i,k}^T : (\mathbf{v}_{i,k}^\tau)^T (\mathbf{S}_k^\tau)^{-1} (\mathbf{v}_{i,k}^\tau) \leq \gamma\}, \quad i = 1, \dots, m_k^\tau, \quad (18)$$

where γ is a gate threshold and m_k^τ is the number of measurements in the gate of the track τ , $\mathbf{v}_{i,k}^\tau = \mathbf{y}_{i,k}^\tau - \bar{\mathbf{y}}_{i,k}^\tau$, is a zero-mean Gaussian residual with covariance \mathbf{S}_k^τ . Given the predicted sample measurements $\mathbf{y}_{k|k-1}^{n,\tau}$ with weights $w_{k-1}^{n,\tau}$ from (24), the predicted measurement $\bar{\mathbf{y}}_{k|k-1}^\tau$ and the innovation covariance \mathbf{S}_k^τ are empirically calculated as

$$\bar{\mathbf{y}}_{k|k-1}^\tau = \sum_{n=1}^N w_{k-1}^{n,\tau} \mathbf{y}_{k|k-1}^{n,\tau}, \quad \mathbf{y}_{k|k-1}^{n,\tau} = h_k(\mathbf{x}_{k|k-1}^{n,\tau}) \quad (19)$$

$$\mathbf{S}_k^\tau = \sum_{n=1}^N w_{k-1}^{n,\tau} (\mathbf{y}_{k|k-1}^{n,\tau} - \bar{\mathbf{y}}_{k|k-1}^\tau)(\mathbf{y}_{k|k-1}^{n,\tau} - \bar{\mathbf{y}}_{k|k-1}^\tau)^T.$$

Given the gated measurements, we exploit amplitude thresholding to filter out false alarms with the threshold DT because the amplitude from a target is usually stronger than false alarms [2].

Then, we select the amplitude with the maximum strength in the set and consider it as a_k^τ . Therefore, we consider the measurement with the strongest amplitude in the gate as a target originated one, which is similar to the strongest neighbour association [6].

However, we also found out that strongest neighbour data association [6], which does not use the spatial measurement, causes tracking performance degradation when associating measurements with tracks. Furthermore, exploiting only the spatial measurements for track-to-measurement association significantly reduces performance in comparison to the performance achieved when both measurements are used. We provide more details of the experimental comparison results in Section 4.3. Therefore, in this paper, we use spatial and amplitude measurements to improve the association accuracy between tracks and measurements, and we present an effective association method, which uses both features, in the following section.

3.3 Data association

We briefly discuss LMIPDA-AI and refer to [21] for further details. We consider the following two association events:

- $\chi_{0,k}^\tau$: None of measurements are associated with track τ .
- $\chi_{i,k}^\tau$: The measurement $z_{i,k}^\tau$ is associated with track τ .

The posterior association probabilities for both events $\chi_{0,k}^\tau$ and $\chi_{i,k}^\tau$ can be evaluated by

$$\beta_{i,k}^\tau = \begin{cases} \frac{P(\chi_{0,k}^\tau | \mathcal{Z}^k, M_k)}{P(\chi_k^\tau | \mathcal{Z}^k, M_k)} = \frac{1 - P_D^\tau P_G^\tau}{1 - \Psi_k^\tau}, & i = 0, \\ \frac{P(\chi_{i,k}^\tau | \mathcal{Z}^k, M_k)}{P(\chi_k^\tau | \mathcal{Z}^k, M_k)} = \frac{P_D^\tau P_G^\tau}{1 - \Psi_k^\tau} \cdot \frac{\Lambda_{i,k}^\tau}{\Phi_{i,k}^\tau}, & i = 1, \dots, m_k^\tau, \end{cases} \quad (20)$$

where P_D^τ and P_G^τ are the target detection and gate probabilities, respectively.

Then, using the spatial and amplitude features, the likelihood model $\Lambda_{i,k}^\tau$ can be acquired based on the assumption of independent spatial measurement $y_{i,k}^\tau$ and amplitude measurement $a_{i,k}^\tau$. Consequently, $\Lambda_{i,k}^\tau$ is derived such that

$$\Lambda_{i,k}^\tau \equiv p(\mathbf{z}_{i,k}^\tau | \chi_k^\tau, \mathcal{Z}^{k-1}) = p(\mathbf{y}_{i,k}^\tau | \chi_k^\tau, \mathbb{Y}^{k-1}) \times p(a_{i,k}^\tau | \chi_k^\tau, \mathbb{A}^{k-1}) = \Lambda_{i,k}^{p,\tau} \cdot \Lambda_{i,k}^{a,\tau}, \quad (21)$$

where the spatial likelihood function $\Lambda_{i,k}^{p,\tau}$ and the amplitude likelihood function $\Lambda_{i,k}^{a,\tau}$ become

$$\Lambda_{i,k}^{p,\tau} = \mathcal{N}(\mathbf{v}_{i,k}^\tau, \mathbf{S}_k^\tau) = \frac{1}{(2\pi)^{L/2} |\mathbf{S}_k^\tau|^{L/2}} \exp\left(-\frac{1}{2} (\mathbf{v}_{i,k}^\tau)^\top (\mathbf{S}_k^\tau)^{-1} \mathbf{v}_{i,k}^\tau\right), \quad (22)$$

$$\Lambda_{i,k}^{a,\tau} = g_a^{\text{DT}}(a_{i,k}^\tau | \hat{d}_k^\tau)$$

Note that the estimated SNR \hat{d}_k^τ can be obtained by solving (15) or (17). The innovation covariance \mathbf{S}_k^τ and the residual $\mathbf{v}_{i,k}^\tau$ of the track is computed using (19)

$$\Psi_k^\tau = P_D^\tau P_G^\tau \cdot \left(1 - \sum_{i=1}^{m_k^\tau} \frac{\Lambda_{i,k}^\tau}{\Phi_{i,k}^\tau}\right)$$

is obtained using the target likelihood (21) and scatterer [21] models. $\Phi_{i,k}^\tau$ is probability that measurement $z_{i,k}^\tau$ is originated from scatterer [21]. The track existence probability is predicted and updated as

$$\text{Predict: } P(\chi_k^\tau | \mathcal{Z}^{k-1}) = \alpha_{11} P(\chi_{k-1}^\tau | \mathcal{Z}^{k-1}) + \alpha_{21} (1 - P(\chi_{k-1}^\tau | \mathcal{Z}^{k-1})),$$

$$\text{Update: } P(\chi_k^\tau | \mathcal{Z}^k) = \frac{(1 - \Psi_k^\tau) \cdot P(\chi_k^\tau | \mathcal{Z}^{k-1})}{1 - \Psi_k^\tau \cdot P(\chi_k^\tau | \mathcal{Z}^{k-1})}. \quad (23)$$

where transition probabilities $\alpha_{11} \equiv P(\chi_k^\tau | \chi_{k-1}^\tau)$ and $\alpha_{21} \equiv P(\chi_k^\tau | \bar{\chi}_{k-1}^\tau)$ are set to 0.98 and 0.02, respectively.

3.4 Track state update

In this section, we propose a Monte Carlo filtering method to estimate the states of multiple targets, where the behaviours of the targets can be modelled by either linear or non-linear dynamic models.

Given a motion model $p(\mathbf{x}_k^\tau | \mathbf{x}_{k-1}^\tau)$ and a likelihood model $p(\mathbf{z}_k^\tau | \mathbf{x}_k^\tau)$, the Monte Carlo filter (or particle filter) [17] performs the prediction and update steps. To deal with complicated distributions which are analytically intractable, we approximate these two steps using a set of weighted samples $\{\mathbf{x}_k^{n,\tau}, w_k^{n,\tau}\}_{n=1}^N$, where N is the number of particles.

When measurements $\mathbf{z}_{1:k}^\tau$ of the track τ up to scan k are provided, all states of the target up to scan k (i.e. trajectory) $\mathbf{x}_{1:k}^\tau$ can be updated well by the prediction-update steps. In most MTT scenarios, however, it is not easy to identify origin of measurements because the detection responses are often unreliable (e.g. false positive, missing and inaccurate detections) and the responses of other targets are present. To update the states of a track with unreliable measurements, we need to select a measurement z_k^τ corresponding to the track τ in the set \mathcal{Z}_k . In this

work, we select z_k^τ among $\mathcal{Z}_k^\tau = \{z_{i,k}^\tau\}_{i=1}^{m_k^\tau}$ according to the posterior association probability $\beta_{i,k}^\tau$ (20). More specifically, when the number of particles is $N = 100$, 100 measurements are generated by random selection in the set \mathcal{Z}_k^τ according to $\beta_{i,k}^\tau$. This procedure is rather similar to resampling in particle filtering: a measurement with a high value $\beta_{i,k}^\tau$ is more likely to be selected in the set. By incorporating this measurement selection step, we extend the two-step recursion of the conventional particle filtering to a three-step procedure as follows:

$$\begin{aligned} \text{Predict: } p(\mathbf{x}_k^\tau | \mathbf{z}_{1:k-1}^\tau) &= \int p(\mathbf{x}_k^\tau | \mathbf{x}_{k-1}^\tau) p(\mathbf{x}_{k-1}^\tau | \mathbf{z}_{1:k-1}^\tau) d\mathbf{x}_{k-1}^\tau, \\ \text{Select: } z_k^\tau &\sim \beta_{i,k}^\tau, \quad z_k^\tau \in \{z_{i,k}^\tau\}_{i=1}^{m_k^\tau}, \\ \text{Update: } p(\mathbf{x}_k^\tau | \mathbf{z}_{1:k}^\tau) &\propto p(z_k^\tau | \mathbf{x}_k^\tau) p(\mathbf{x}_k^\tau | \mathbf{z}_{1:k-1}^\tau). \end{aligned} \quad (24)$$

In our experiment, we found that the proposed filtering method shows the similar performance with the particle filtering using probabilistic data association [22], but it has much low complexity $O(N)$ compared to the complexity $O(Nm_k^\tau)$ of [22].

4 Simulation results and discussion

In this section, we evaluate the proposed system by comparing it with other MTT systems for various tracking scenarios.

4.1 Implementation and evaluation metric

To verify the effectiveness of the proposed system shown in Fig. 3, we implemented tracking systems as described in Table 2 (all with particle filtering): system (s1) associates a measurement with the strongest amplitude in each track gate as in [6], whereas system (s2) only uses spatial measurements (i.e. range and bearing) without amplitude measurements. Systems (s3)–(s6) use both measurements. In system (s3), we use the SNRs of targets, but we do not use them in systems (s4)–(s6). Since no SNRs are available,

system (s4) designs the amplitude likelihood function (10) using the marginalisation method [2]. On the other hand, systems (s5) and (s6) model the function by estimating SNRs with amplitude measurements, but in different ways. While system (s5) employs the SMC method [21], system (s6) uses the proposed MAP method.

As a performance measure, we use the optimal subpattern assignment (OSPA) metric [23]. Given the true and estimated sets composed of states of multiple targets, we measure the OSPA distance by summing both the localisation and cardinality distances. The cut-off parameter and the order parameter then are set to 100 and 1.

4.2 Experimental MTT scenarios

To evaluate the performance of the implemented systems (s1)–(s6), we generated three MTT scenarios with various dynamic motion models and experimental conditions.

Trajectory generation: As shown in Figs. 4a–c, we generate the target trajectories over 500 scans. The (nearly) constant velocity model [24] is used for scenarios I and II. To assess our system under more challenging conditions, the constant turn model [24] is used in scenario III [The initial parameters of the targets and surveillance time are presented in Table 1 of the Supplementary material. For all the scenarios, the SNRs randomly fluctuate according to (16) with a variance $\Sigma_\zeta = 10$. Note that these parameters are not provided to trackers in evaluation.].

Measurement generation: At each scan k , a set of target originated measurements containing the range, bearing and amplitude components are generated with the detection probability $P_D = 0.8$. Each component is polluted by the additive white Gaussian noise with standard deviations 3.16 m, 1.4° and 1, respectively. According to the Rayleigh distribution (6), the amplitudes of targets are determined with their SNRs.

The sensor detection region considered has a radial distance range [0 m, 1000 m] and angle range [0°, 360°]. Within the detection region, clutter is uniformly distributed. The amount of the clutter is controlled by the clutter density λ (measurements/scan/m²). We set the $\lambda = 3 \times 10^{-5}$, $\lambda = 5 \times 10^{-5}$ and $\lambda = 10^{-4}$, resulting in 30, 50 and 100 clutter detections per scan, respectively. Figs. 4d–o present all detected measurements over 500 scans.

Tracking parameters: As a proposal density used for propagating samples, we simply use the transitional prior motion $p(\mathbf{x}_k^r | \mathbf{x}_{k-1}^r) = \mathcal{N}(\mathbf{x}_k^r; f(\mathbf{x}_{k-1}^r), \mathbf{Q}_k^r)$, $\mathbf{Q}_k^r = \Gamma_k \mathbf{Q}_k \Gamma_k^T$, where f is in general non-linear transfer function, Γ_k is the noise gain matrix, and the noise covariance is set to $\mathbf{Q}_k = \text{diag}[10(\text{m/s})^2, 10(\text{m/s})^2]^T$. The noise covariance is significantly different from the true covariance $\mathbf{Q}_k = \text{diag}[1(\text{m/s})^2, 1(\text{m/s})^2]^T$ used to generate the target trajectories. This different setup is intended to investigate whether the proposed system still performs well when the exact dynamic motion is not available.

Using the track initialisation method [1], the initial states of tracks are determined with associated measurements during few recent scans. For all experiments, the initial covariance is set to $\mathbf{P}_k^r = \text{diag}[1 \text{ m}^2, 25(\text{m/s})^2, 1 \text{ m}^2, 25(\text{m/s})^2]^T$ in the consideration of maximum velocities of moving targets.

Table 2 Implemented MTT systems for the performance evaluation

Filters	Description
(s1) SND	strongest neighbour data association [6]
(s2) LMIPDA	without amplitude measurement
(s3) LMIPDA-AI-SNR	with known SNR
(s4) LMIPDA-AI-MRG	unknown SNR estimation with the marginalisation method [2]
(s5) LMIPDA-AI-SMC	unknown SNR estimation using the sequential Monte Carlo method [21]
(s6) LMIPDA-AI-MAP	unknown SNR estimation using the proposed method

To make a fair assessment, systems (s1)–(s6) all exploit the same measurements and the same number of samples $N = 100$. The thresholds of gate and amplitude are tuned by $\gamma = 15$ and $DT = 0.7$. For marginalisation of the amplitude likelihood function in system (s3), the SNR range boundary is 0–30 dB, similar that in to [2]. In system (s4), the SNR is sequentially estimated using the SMC method with the uniform proposal density function [21].

4.3 Evaluation results

For the three MTT scenarios, Table 3 compares the performance of systems (s1)–(s6) in terms of the OSPA metric. We compute mean errors (*or* distance) and standard deviation by using the evaluation results for 500 scans and 500 Monte Carlo runs as shown in Table 3A–C. Moreover, we provide the computational costs per scan in Table 3D.

In general, the OPSA errors of all systems slightly increase when the number of targets is large, and their motions are complex, such as in scenario III. We found that the system performance can be significantly enhanced by incorporating amplitude information. For all OSPA errors Table 3A–C in all scenarios, systems (s1) and (s3)–(s6) using amplitude show better performance than system (s2), which does not utilise amplitude information. In particular, the performance difference becomes larger as the clutter density becomes higher, i.e. $\lambda = 1 \times 10^{-4}$ measurements/scan/m². Based on this comparison, we confirm that the amplitude truly help trackers to discriminate between the target and clutter responses more clearly.

System (s1) based on SND directly uses amplitude information for track-to-measurement association. On the other hand, for the association, systems (s3) and (s5)–(s6), which are based on LMIPDA-AI, employ spatial measurements as well as amplitudes. When the clutter density is low, system (s1) shows performance similar to systems (s3), and (s5)–(s6). However, systems (s3) and (s5)–(s6) show better performance than system (s1) when clutter densities are increased [The performance gap is obvious in Table 4.]. The main reason is that more clutter measurements with high amplitudes are generated within the gates as the clutter density increases. As a result, system (s1) is likely to associate a clutter measurement with a high amplitude.

However, systems (s3) and (s5)–(s6) based on the LMIPDA-AI do not degrade the tracking performance since they exploit both spatial and amplitude features when evaluating likelihoods (21). As a result, even though a clutter measurement has the highest amplitude in a gate, the total likelihood can be reduced when either their spatial likelihood is low. In addition, we consider the statistical properties of amplitude and SNR for amplitude likelihood evaluation (22). Therefore, their likelihood can be low even when the highest amplitude does not match well with the estimated target SNR in the density (4).

In Fig. 5, we further provide the more comparison results of association accuracies of tracking systems with different types of measurements based on 500 Monte Carlo runs. To evaluate their association accuracy, we first select a measurement within the gate and then investigate whether the selected one comes from a target or not. As expected, the accuracy of system (s6) using both measurements is superior to systems (s1) and (s2).

When the SNR is unknown, Table 3 shows that the performance of systems (s5) and (s6), which use the estimated SNR, is superior to the performance of system (s4). In particular, the cardinality error is very low in all scenarios, as shown in Table 3B. One possible explanation is that more false alarms and fewer true measurements are thresholded out with the likelihood function by using the estimated SNR information. Moreover, the comparison between systems (s5) and (s6) demonstrates that system (s6), which uses the proposed method for SNR estimation, performs better than system (s5).

The computational complexity of systems (s1)–(s6) is presented in Table 3D. Comparison of system (s2) with systems (s1), (s3)–(s6) shows that the computation time can be considerably reduced (almost 30–55%) when amplitude information is used. In particular, employing amplitude information offers greater cost benefits when more clutter measurements exist. Furthermore, the

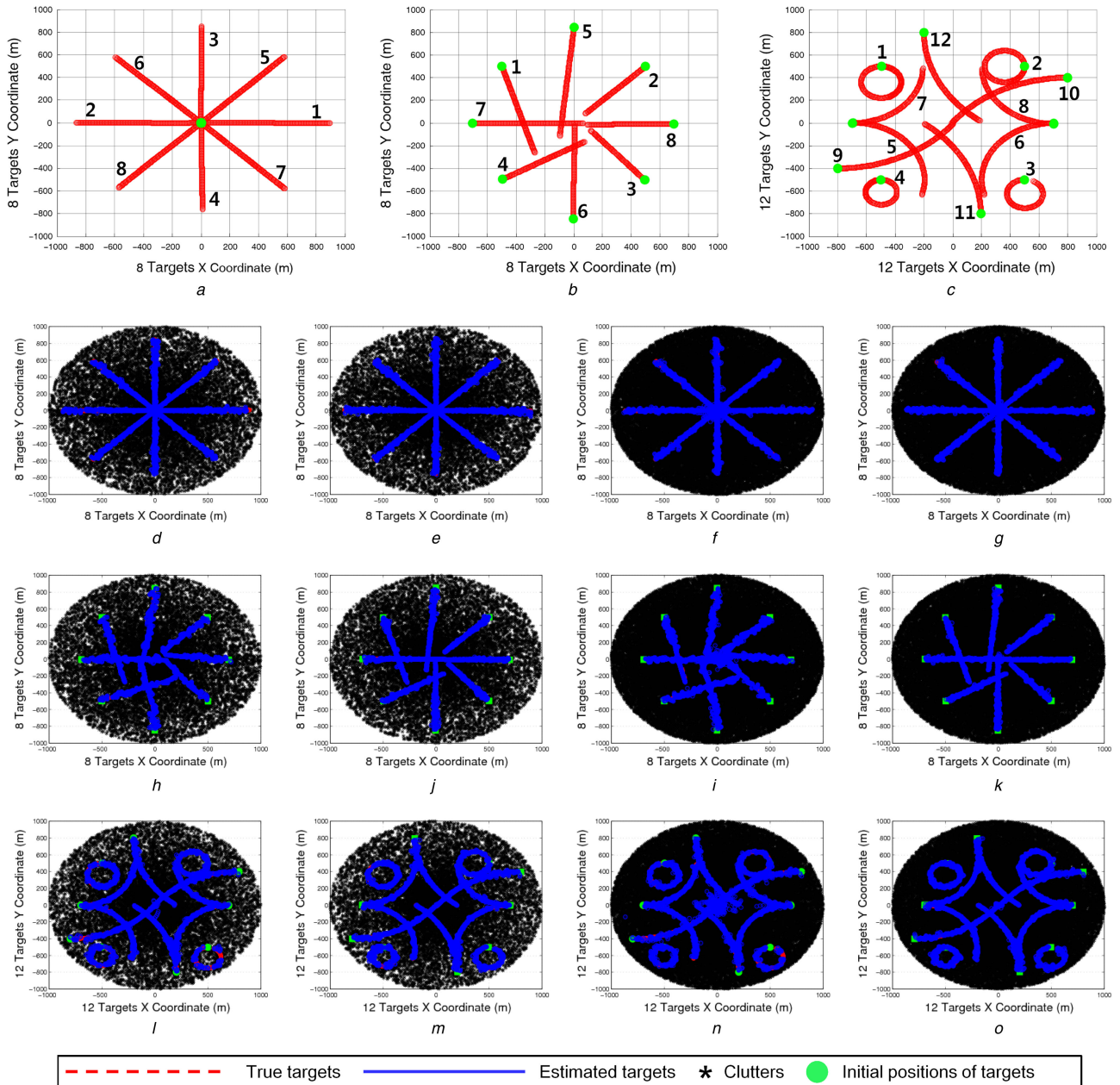


Fig. 4 For the three MTT scenarios, trajectories of the true targets (thick lines in a-c) and the corresponding estimated targets (thick lines in d-o) are illustrated. We then compare the performance of systems (s2) and (s6) under different clutter densities

(a) Scenario I: True trajectories, (b) Scenario II: True trajectories, (c) Scenario III: True trajectories, (d) System (s2) and $\lambda = 3 \times 10^{-5}$, (e) System (s6) and $\lambda = 3 \times 10^{-5}$, (f) System (s2) and $\lambda = 10^{-4}$, (g) System (s6) and $\lambda = 10^{-4}$, (h) System (s2) and $\lambda = 3 \times 10^{-5}$, (i) System (s6) and $\lambda = 3 \times 10^{-5}$, (j) System (s2) and $\lambda = 10^{-4}$, (k) System (s6) and $\lambda = 10^{-4}$, (l) System (s2) and $\lambda = 3 \times 10^{-5}$, (m) System (s6) and $\lambda = 3 \times 10^{-5}$, (n) System (s2) and $\lambda = 10^{-4}$, (o) System (s6) and $\lambda = 10^{-4}$

results demonstrate that the computational cost is not significantly increased by the proposed system (s6), and they verify the effectiveness of the proposed algorithm.

The tracking results for the three MTT scenarios with different clutter densities are shown in Fig. 4. We can observe that the trajectories constructed by system (s6) are clearer than those constructed by system (s2) due to the existence of fewer false tracks. When the amplitude is not used, too many false tracks are generated, as shown in Figs. 4f, j and n. This phenomenon is especially distinct in scenario III, in which many targets move in a complex dynamic motion.

These results demonstrate that the proposed SNR estimation algorithm accurately estimates unknown target SNRs and significantly improves the data association performance. Thus, the proposed method allows us to boost the overall performance of the MTT system.

4.4 Evaluation using pedestrian dataset

To evaluate the performance of our system in real scenarios, we used the publicly available PETS S2.L1 sequence consisting of 795 frames [25] shown in Fig. 6a. The sequence is very challenging due to the abrupt motion changes of targets and the frequent occlusion of targets and scene clutter. Similar to the previous experiment, we allocated the targets to different initial SNRs. At each frame, we made the target SNRs randomly fluctuate using (16) with a variance $\Sigma_{\zeta} = 10$ and generated clutter with various clutter densities of $\lambda = 8.2 \times 10^{-5}$, $\lambda = 1.6 \times 10^{-4}$ and $\lambda = 2.5 \times 10^{-4}$ (measurements/frame/pixel²) [The initial states of the targets and their surveillance time are given in Table 2 of the supplementary material.].

As discussed in Section 4.2, the same tracking parameters were also used for implementation except for the covariance \mathbf{Q}_k , where $\mathbf{Q}_k = \text{diag}[5(\text{pixel}/\text{frame})^2 \ 5(\text{pixel}/\text{frame})^2]^T$ by considering the frame rate. We compared the tracking performance of systems

Table 3 For the three MTT scenarios, the time-averaged results of the OSPA metric (mean errors/standard deviation) between sets of the true and estimated states under different clutter densities for systems (s1)–(s6) are evaluated based on 500 Monte Carlo simulations. Also, the computational time per scan is calculated by averaging running time during 500 scans

Clutter density λ (measurements/scan/m ²)	MTT systems					
	(s1)-SND	(s2)-w/o amplitude	(s3)-known SNR	(s4)-marginalisation	(s5)-SMC	(s6)-proposed
Scenario I						
(A) OSPA distance						
3×10^{-5}	20.858/3.044	21.570/1.851	17.522/2.764	28.264/4.131	27.988/4.138	18.192/2.577
5×10^{-5}	23.173/2.201	22.568/1.616	17.364/2.238	28.278/4.095	28.107/4.066	18.870/1.828
1×10^{-4}	33.366/1.278	31.095/1.317	17.384/2.297	28.712/3.522	28.312/3.524	19.479/1.532
(B) OSPA cardinality						
3×10^{-5}	13.346/2.857	14.227/1.643	10.083/2.719	22.675/4.024	22.319/3.996	10.224/2.514
5×10^{-5}	13.657/2.022	13.274/1.419	9.773/2.096	22.681/4.042	22.407/4.001	10.809/1.739
1×10^{-4}	20.870/1.263	18.102/1.233	9.740/2.187	22.554/3.500	22.084/3.466	10.880/1.436
(C) OSPA localisation						
3×10^{-5}	7.511/0.161	7.342/0.153	7.438/0.148	5.588/0.055	5.669/0.058	7.968/0.188
5×10^{-5}	9.515/0.317	9.294/0.312	7.591/0.146	5.597/0.054	5.700/0.056	8.061/0.186
1×10^{-4}	12.496/0.737	12.992/0.811	7.644/0.150	6.158/0.057	6.228/0.058	8.599/0.181
(D) Computational time						
3×10^{-5}	0.0389	0.0408	0.0386	0.0390	0.0396	0.0617
5×10^{-5}	0.0505	0.0556	0.0515	0.0501	0.0507	0.0666
1×10^{-4}	0.0998	0.1081	0.0960	0.0993	0.1011	0.0775
Scenario II						
(A) OSPA distance						
3×10^{-5}	14.951/3.744	15.534/3.876	14.058/3.446	14.618/3.592	14.665/3.614	13.464/2.319
5×10^{-5}	16.486/3.602	19.155/3.691	14.114/3.445	14.850/3.391	14.861/3.382	13.562/2.058
1×10^{-4}	21.434/3.757	27.029/3.444	14.514/3.416	16.637/3.354	16.465/3.336	15.759/2.008
(B) OSPA cardinality						
3×10^{-5}	8.283/3.566	9.049/3.657	7.746/3.450	8.201/3.517	8.224/3.516	6.462/1.982
5×10^{-5}	9.175/3.397	11.220/3.442	7.774/3.462	8.247/3.377	8.247/3.370	6.689/1.928
1×10^{-4}	12.257/2.769	16.215/2.264	8.088/3.423	9.430/3.426	9.370/3.422	8.496/1.919
(C) OSPA localisation						
3×10^{-5}	6.668/0.197	6.484/0.171	6.311/0.134	6.417/0.159	6.441/0.166	7.002/0.206
5×10^{-5}	7.310/0.209	7.934/0.279	6.340/0.135	6.603/0.139	6.613/0.139	6.873/0.136
1×10^{-4}	9.177/0.707	10.814/1.550	6.425/0.140	7.207/0.190	7.094/0.176	7.262/0.163
(D) Computational time						
3×10^{-5}	0.0345	0.0366	0.0343	0.0344	0.0346	0.0559
5×10^{-5}	0.0465	0.0499	0.0452	0.0457	0.0463	0.0595
1×10^{-4}	0.0931	0.1019	0.0898	0.0917	0.0920	0.0699
Scenario III						
(A) OSPA distance						
3×10^{-5}	29.579/2.842	29.855/2.971	19.995/2.397	34.694/3.069	20.840/2.695	20.145/2.315
5×10^{-5}	31.497/3.144	31.696/3.143	20.063/2.403	34.745/2.965	21.573/2.775	20.877/2.379
1×10^{-4}	37.912/3.309	37.299/3.273	20.110/2.350	34.540/2.916	21.701/2.431	20.935/2.269
(B) OSPA cardinality						
3×10^{-5}	19.864/2.560	21.207/2.798	11.393/2.463	27.745/3.038	11.998/2.499	10.757/2.196
5×10^{-5}	18.949/3.029	20.230/3.149	11.375/2.461	27.667/2.959	12.624/2.608	11.244/2.283
1×10^{-4}	16.840/2.612	16.242/2.506	11.369/2.423	27.389/2.964	11.881/2.090	10.901/2.061
(C) OSPA localisation						
3×10^{-5}	9.715/0.470	8.648/0.304	8.601/0.116	6.948/0.158	8.842/0.212	9.388/0.173
5×10^{-5}	12.548/0.513	11.466/0.338	8.687/0.121	7.077/0.159	8.948/0.235	9.633/0.205
1×10^{-4}	21.071/0.961	21.057/1.126	8.740/0.118	7.150/0.144	9.819/0.220	10.034/0.173
(D) Computational time						
3×10^{-5}	0.0520	0.0542	0.0514	0.0521	0.0522	0.0837
5×10^{-5}	0.0660	0.0705	0.0647	0.0658	0.0659	0.0866
1×10^{-4}	0.1187	0.1291	0.1149	0.1181	0.1167	0.1007

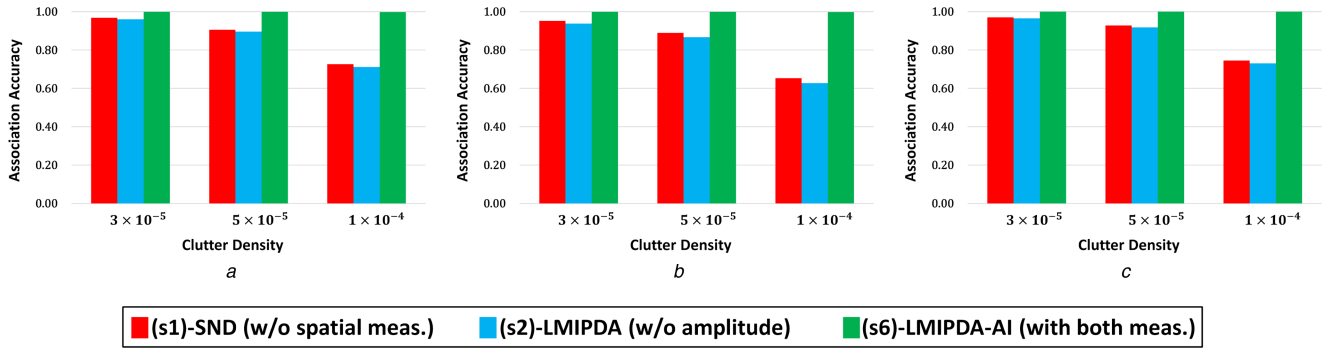


Fig. 5 For three MTT scenarios, association performance of systems using different features is evaluated based on 500 Monte Carlo runs (a) Scenario I, (b) Scenario II, (c) Scenario III

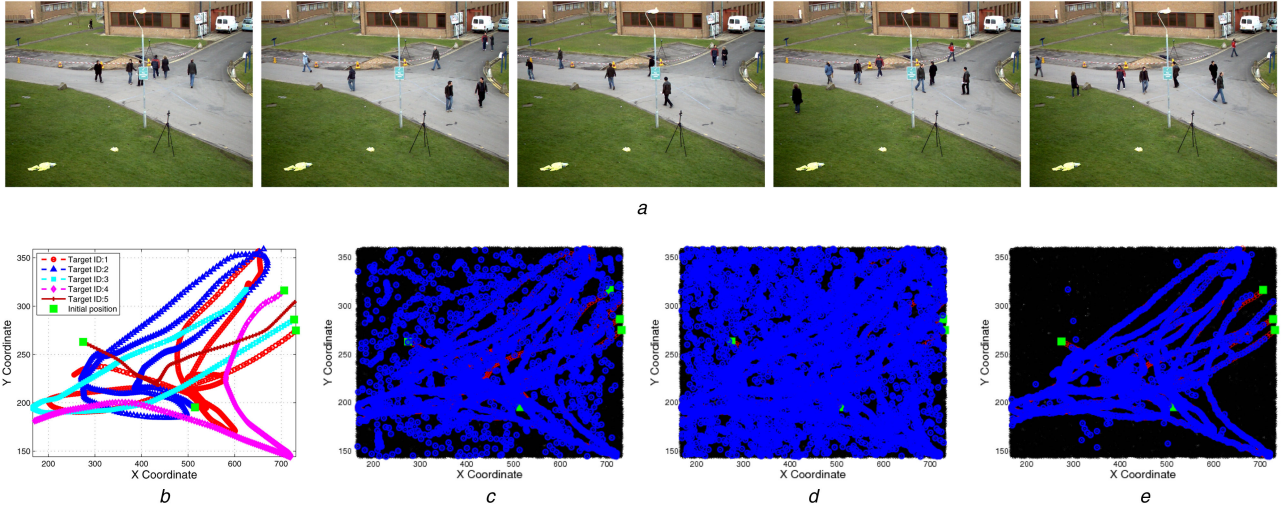


Fig. 6 True and estimated trajectories with different tracking systems for the PETS-L1 sequence [25] over 795 frames (a) PETS-L1 tracking sequences (from left to right): frame 86, frame 192, frame 273, frame 716, frame 740, (b) True trajectories, (c) (s1) and $\lambda = 2.5 \times 10^{-4}$, (d) (s2) and $\lambda = 2.5 \times 10^{-4}$, (e) (s6) and $\lambda = 2.5 \times 10^{-4}$

(s1)–(s6) in terms of the OSPA metric and the results are shown in Table 4. System (s6) with the proposed SNR estimation method shows the better performance than systems (s1), (s2), (s4), and

(s5). Figs. 6c–e show the constructed trajectories. When clutter is densely distributed, systems (s1) and (s2) produce too many false

Table 4 For the VS-PETS 2009 dataset, the time-averaged results of the OSPA metric (mean errors/standard deviation) between sets of the true and estimated states under different clutter densities for systems (s1)–(s6) are evaluated based on 500 Monte Carlo simulations. Also, the computational time per frame is calculated by averaging running time during 795 frames

Clutter density λ (measurements/scan/m ²)	MTT systems					
	(s1)-SND	(s2)-w/o amplitude	(s3)-known SNR	(s4)-marginalization	(s5)-SMC	(s6)-proposed
VS-PETS 2009 dataset						
(A) OSPA distance						
8.2×10^{-5}	11.796/3.509	14.696/2.207	7.835/1.530	16.539/3.635	14.412/1.581	6.179/1.479
1.6×10^{-4}	16.883/3.338	23.867/2.639	11.034/1.360	14.730/3.739	13.953/1.450	11.896/1.365
2.5×10^{-4}	41.811/2.396	67.173/1.194	9.391/1.399	17.657/4.089	14.697/1.507	10.193/1.339
(B) OSPA cardinality						
8.2×10^{-5}	9.768/3.216	13.076/2.050	6.467/1.504	14.386/3.445	12.642/1.549	4.866/1.415
1.6×10^{-4}	13.480/2.761	22.087/2.593	9.312/1.280	12.754/3.509	12.067/1.371	10.026/1.254
2.5×10^{-4}	38.145/2.534	66.297/1.244	7.578/1.304	15.469/3.944	12.596/1.413	8.198/1.227
(C) OSPA localisation						
8.2×10^{-5}	2.027/0.033	1.620/0.145	1.367/0.057	2.153/0.160	1.769/0.066	1.312/0.057
1.6×10^{-4}	3.403/0.277	1.780/0.184	1.722/0.034	1.976/0.077	1.886/0.059	1.870/0.043
2.5×10^{-4}	3.665/0.447	0.875/0.041	1.813/0.047	2.188/0.105	2.101/0.106	1.994/0.078
(D) Computational time						
8.2×10^{-5}	0.0123	0.0141	0.0145	0.0137	0.0152	0.0273
1.6×10^{-5}	0.0174	0.0216	0.0162	0.0168	0.0175	0.0312
2.5×10^{-4}	0.0345	0.0524	0.0263	0.0315	0.0298	0.0390

tracks and inaccurate tracks. On the other hand, the proposed system (s6) successfully constructs long trajectories.

5 Conclusion

In many practical scenarios, target SNRs randomly fluctuate. To estimate the changed SNRs, we proposed a novel SNR estimation method via the ML and MAP inference. We further designed an MTT framework consisting of data association and track state update parts using the estimated SNR. The extensive evaluation results confirm that the proposed methods can estimate SNRs and significantly improve the performance of the MTT system.

6 Acknowledgment

This work was supported by Institute for Information & communications Technology Promotion (IITP) grant funded by the Korea government (MSIP) (No. B0101-15-0266, Development of High Performance Visual BigData Discovery Platform for Large-Scale Realtime Data Analysis) and the National Research Foundation of Korea (NRF) grant funded by the Korea government (MSIP) (No. NRF-2015R1A2A1A01005455).

7 References

- [1] Bar-Shalom, Y.: *Multitarget-multisensor tracking: applications and advances* (Artech House, 1990), pp. 25–42
- [2] Clark, D., Ristic, B., Vo, B.-N., *et al.*: ‘Bayesian multi-object filtering with amplitude feature likelihood for unknown object SNR’, *IEEE Trans. Signal Process.*, 2010, **58**, (1), pp. 26–37
- [3] Yildirim, M.E., Ince, I.F., Salman, Y.B., *et al.*: ‘Direction-based modified particle filter for vehicle tracking’, *ETRI J.*, 2016, **38**, (2), pp. 356–365
- [4] Choi, J.W., Moon, D., Yoo, J.H.: ‘Robust multi-person tracking for real-time intelligent video surveillance’, *ETRI J.*, 2015, **37**, (3), pp. 551–561
- [5] Bar-Shalom, Y., Li, X.R.: *Multitarget-multisensor tracking: principles and techniques* (YBS Publishing, Storrs, CT, 1995)
- [6] Li, X.R.: ‘Tracking in clutter with strongest neighbor measurements. Part I: Theoretical analysis’, *IEEE Trans. Autom. Control*, 1998, **43**, (11), pp. 1560–1578
- [7] Reid, D.: ‘An algorithm for tracking multiple targets’, *IEEE Trans. Autom. Control*, 1979, **24**, (6), pp. 843–854
- [8] Mušicki, D., La Scala, B.: ‘Multi-target tracking in clutter without measurement assignment’, *IEEE Trans. Aerosp. Electron. Syst.*, 2008, **44**, (3), pp. 877–896
- [9] Cho, J.A., Na, H.B., Kim, S.W., *et al.*: ‘Moving-target tracking based on particle filter with TDOA/FDOA measurements’, *ETRI J.*, 2012, **34**, (2), pp. 260–263
- [10] Kim, D.S., Song, T.L., Mušicki, D.: ‘Highest probability data association for multi-target particle filtering with nonlinear measurements’, *IEICE Trans. Commun.*, 2013, **E96-B**, (1), pp. 281–290
- [11] La Scala, B.F.: ‘Viterbi data association tracking using amplitude information’ Seventh Int. Conf. on Information Fusion, Stockholm, Sweden, June–July 2004
- [12] Lerro, D., Bar-Shalom, Y.: ‘Automated tracking with target amplitude information’ American Control Conf., 1990, pp. 2875–2880
- [13] Van Keuk, G.: ‘Multihypothesis tracking using incoherent signal-strength information’, *IEEE Trans. Aerosp. Electron. Syst.*, 1996, **32**, (3), pp. 1164–1170
- [14] Slocumb, B.J., Klusman, M.E.: ‘A multiple Model SNR/ RCS likelihood ratio score for radar-based feature-aid tracking’. Proc. SPIE. Signal and Data Processing of Small Targets, San Diego, CA, USA, 2 August 2005, vol. **5913**
- [15] Swerling, P.: ‘Probability of detection for fluctuating target’, *IRE Trans. Inf. Theory*, 1960, **58**, (1), pp. 26–37
- [16] Skolnik, M.I.: *Introduction to radar system* (McGraw-Hill, New York, 2002, 3rd edn.)
- [17] Arulampalam, M.S., Maskell, S., Gordon, N., *et al.*: ‘A tutorial on particle filters for non-linear/non-Gaussian Bayesian filtering’, *IEEE Trans. Signal Process.*, 2002, **50**, (2), pp. 174–188
- [18] Field, E., Lewinsein, M.: ‘Amplitude-probability distribution model for VLF/ELF atmospheric noise’, *IEEE Trans. Commun.*, 1978, **26**, (1), pp. 83–87
- [19] Nocedal, J., Wright, S.J.: *Numerical optimization* (Springer-Verlag, NewYork, 2006)
- [20] Poli, A.A., Cirillo, M.C.: ‘On the use of the normalized mean square error in evaluation dispersion model performance’, *Atmos. Environ.*, 1993, **27**, (15), pp. 2427–2434
- [21] Bae, S.H., Kim, D.Y., Yoon, J.H., *et al.*: ‘Automated multi-target tracking with kinematic and non-kinematic information’, *IET Radar, Sonar Navig.*, 2012, **6**, (4), pp. 272–281
- [22] Ekman, M.: ‘Particle filters and data association for multi-target tracking’. 11th Int. Conf. on Information Fusion, 2008
- [23] Schuhmacher, D., Vo, B.-T., Vo, B.-N.: ‘A consistent metric for performance evaluation of multi-object filters’, *IEEE Trans. Signal Process.*, 2008, **56**, (8), pp. 3447–3457
- [24] Li, X.R., Jilkov, V.P.: ‘Survey of maneuvering target tracking. Part I: Dynamic models’, *IEEE Trans. Aerosp. Electron. Syst.*, 2003, **39**, (4), pp. 1333–1364
- [25] VS-PETS dataset. <http://www.cvg.reading.ac.uk/PETS2009/a.html>